| | |
|---|---|
| Title | Population Pulsation Resonances of Excitons in Monolayer MoSe2 with Sub-1 μeV Linewidths |
| Author(s) | Schaibley, JR; Karin, T; Yu, H; Ross, JS; Rivera, P; Jones, AM; Scott, ME; Yan, J; Mandrus, DG; Yao, W; Fu, KM; Xu, X |
| Citation | Physical Review Letters, 2015, v. 114, p. 137402:1-6 |
| Issued Date | 2015 |
| URL | http://hdl.handle.net/10722/209817 |
| Rights | Physical Review Letters. Copyright © American Physical Society.<br>Creative Commons: Attribution 3.0 Hong Kong License |

# Population Pulsation Resonances of Excitons in Monolayer $MoSe_2$ with Sub-1 $\mu$eV Linewidths

John R. Schaibley,[1] Todd Karin,[1] Hongyi Yu,[2] Jason S. Ross,[3] Pasqual Rivera,[1] Aaron M. Jones,[1] Marie E. Scott,[1] Jiaqiang Yan,[4,5] D. G. Mandrus,[4,5,6] Wang Yao,[2] Kai-Mei Fu,[1,7] and Xiaodong Xu[1,3,*]

[1]*Department of Physics, University of Washington, Seattle, Washington 98195, USA*
[2]*Department of Physics and Center of Theoretical and Computational Physics, University of Hong Kong, Hong Kong, China*
[3]*Department of Materials Science and Engineering, University of Washington, Seattle, Washington 98195, USA*
[4]*Materials Science and Technology Division, Oak Ridge National Laboratory, Oak Ridge, Tennessee 37831, USA*
[5]*Department of Materials Science and Engineering, University of Tennessee, Knoxville, Tennessee 37996, USA*
[6]*Department of Physics and Astronomy, University of Tennessee, Knoxville, Tennessee 37996, USA*
[7]*Department of Electrical Engineering, University of Washington, Seattle, Washington 98195, USA*

(Received 9 December 2014; published 1 April 2015)

Monolayer transition metal dichalcogenides, a new class of atomically thin semiconductors, possess optically coupled 2D valley excitons. The nature of exciton relaxation in these systems is currently poorly understood. Here, we investigate exciton relaxation in monolayer $MoSe_2$ using polarization-resolved coherent nonlinear optical spectroscopy with high spectral resolution. We report strikingly narrow population pulsation resonances with two different characteristic linewidths of 1 and $<0.2$ $\mu$eV at low temperature. These linewidths are more than 3 orders of magnitude narrower than the photoluminescence and absorption linewidth, and indicate that a component of the exciton relaxation dynamics occurs on time scales longer than 1 ns. The ultranarrow resonance ($<0.2$ $\mu$eV) emerges with increasing excitation intensity, and implies the existence of a long-lived state whose lifetime exceeds 6 ns.

DOI: 10.1103/PhysRevLett.114.137402 PACS numbers: 78.20.-e, 78.40.Fy, 78.47.jh

The discovery of the direct band gap nature and unique spin-valley coupled physics in monolayer transition metal dichalcogenides (TMDs) has sparked wide interest in understanding 2D valley excitons [1–3]. These electrically tunable valley excitons allow for direct optical control of spin and valley degrees of freedom, promising for optoelectronics and valleytronics at the atomically thin limit. These applications hinge on the knowledge of key fundamental properties of valley excitons, such as the lifetimes and the intervalley scattering rate, which remain elusive due to the interplay between different excitonic states, inhomogeneous broadening, and many-body interaction effects. Recent progress towards understanding these 2D excitons includes the optical generation of valley exciton polarization and quantum coherence [4–7], electrical tuning of excitonic charging effects [3,7,8], and the identification of exceptionally large exciton [9–15] and trion binding energies [3,8]. However, little is known about the nature of exciton relaxation in TMD monolayers beyond the ultrafast time scale.

In a delocalized 2D excitonic system, the dispersion of the exciton center of mass momentum can be used to classify excitons relative to the photon dispersion, i.e., the light cone [Fig. 1(a)]. Excitons inside of the light cone are referred to as bright excitons, since their center of mass momentum allows them to radiatively recombine. Conversely, dark excitons are located outside of the light cone, and cannot radiatively recombine until they scatter back into the light cone. Therefore, lifetimes for bright excitons are expected to be much shorter than for dark excitons. The presence of dark excitons can add a long lifetime component to the measured exciton decay time. Localized excitons might also exist (e.g., trap or defect-bound states) and could give rise to a long lifetime.

Recent low-temperature time-resolved measurements have shown that a fast component of exciton lifetime is on order of 1–100 ps [16–21] in a variety of TMD monolayer systems. The shortest of these lifetimes are within an order of magnitude of the theoretical predictions for the delocalized bright exciton radiative lifetime [21,22]; however, contributions from dark excitons are expected to significantly increase the measured exciton lifetime [22]. We note that the relatively low quantum yield ($\sim$0.1%) reported thus far in monolayer TMDs [1] appears to conflict with the interpretation that the intrinsic radiative decay is fast, and might imply that nonradiative decay processes dominate the ultrafast exciton relaxation dynamics [23]. To probe these dynamics, techniques other than time resolved pump-probe and photoluminescence can be used to measure longer time scales which are often obscured in ultrafast measurements.

In this Letter, we investigate the low-temperature relaxation rates of valley excitons in monolayer $MoSe_2$ by performing high-resolution coherent nonlinear optical spectroscopy. We report evidence of exciton population dynamics that occur on the nanosecond time scale, which is 1–3 orders of magnitude longer than the lifetimes reported

 

in ultrafast time resolved measurements [16–21]. Our measurements reveal two distinct time scales: (i) a ~1–2 ns lifetime which is associated with the exciton decay time, (ii) and a >6 ns lifetime which we assign to a previously unreported long-lived state. These time scales decrease as exciton density increases, which is evidence of strong many-body interaction effects in 2D semiconductors.

High-resolution coherent nonlinear optical spectroscopy has been used in atomic and solid state systems to probe relaxation processes which are obscured by inhomogeneous broadening and complex relaxation dynamics. In semiconductor optics, this technique was used extensively to study exciton relaxation [24], diffusion [25], and slow light effects [26] of GaAs excitons and nanocrystal systems [27].

We perform a continuous-wave two-color differential reflectivity (DR) measurement which is depicted in Fig. 1(b). Two continuously tunable, narrow bandwidth lasers are used: the pump laser is fixed on the exciton resonance while the probe laser is scanned through zero pump-probe detuning ($\Delta$) at high (<100 neV) resolution. The pump and probe lasers are amplitude modulated at two different frequencies, and a lock-in detection scheme is used to measure the nonlinear optical response at the difference of the modulation frequencies. The laser intensity is sufficiently low so that the dominant contribution to the nondegenerate DR signal is the third-order susceptibility ($\chi^{(3)}$) [Fig. 1(c)].

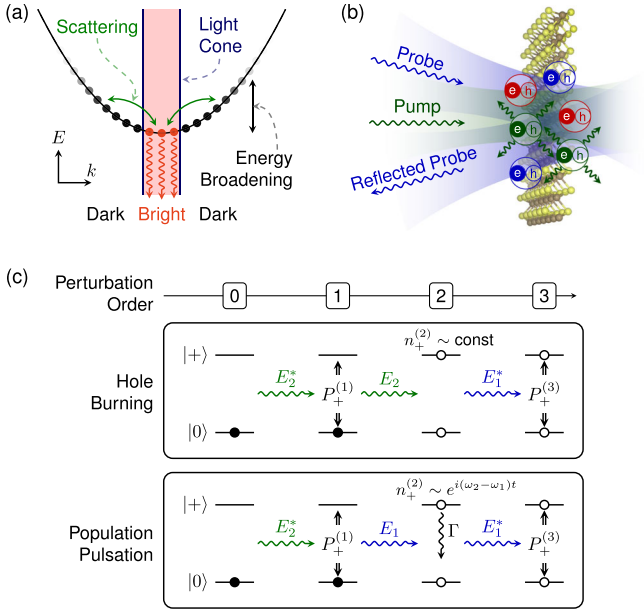


FIG. 1 (color online). (a) Depiction of the dispersion relation for delocalized excitons, where the $x$ axis represents the exciton center of mass momentum. In this picture, only excitons inside of the light cone can efficiently radiatively recombine. (b) Depiction of pump and probe fields interacting with a $MoSe_2$ monolayer. A narrow bandwidth pump laser selectively excites excitons of a particular energy (shown here as green). The interference of the pump and probe laser fields gives rise to a population pulsation resonance. (c) In an inhomogeneous distribution of two-level systems composed of states ($|0\rangle$ and $|+\rangle$), both hole-burning and population pulsation effects can contribute to a $\chi^{(3)}$ response. Here, we show two examples of the perturbation sequence up to third order in the applied fields. $E_1$ and $E_2$ are the probe and pump fields at frequencies $\omega_1$ and $\omega_2$, respectively. $P_+$ is the polarization, and $n_+$ is the excited state population. The superscripts label the perturbation order. The population pulsation effect results in a modulation of the state populations at the pump-probe difference frequency.

The data reported in the main text are from a single $MoSe_2$ monolayer on a $SiO_2$ substrate measured at 30 K. All experiments were performed in the reflection geometry with a beam diameter of about 1.5 $\mu$m. To characterize the sample, we first measure the degenerate DR response by scanning a single laser (split into pump and probe) in energy [Fig. 2(a)]. Comparing the DR response to the photoluminescence spectrum [Fig. 2(a) inset], the DR resonances are assigned to the neutral and charged excitons at 1.655 and 1.625 eV, respectively [3]. This DR signal potentially contains contributions from phase-space filling, exciton-exciton interactions, band gap renormalization by free carriers [28], and excitation-induced dephasing [29]. Optical interference between the sample and substrate [30] also contributes to the asymmetry of the DR line shape by mixing the real and imaginary parts of the electric susceptibility.

In contrast to the few meV linewidth of the degenerate DR spectra, the high resolution two-color DR measurements show narrow ($\mu$eV) resonances, on top of a broad nonlinear signal which approximately follows the degenerate DR spectrum [Fig. 2(a)]. Additional DR

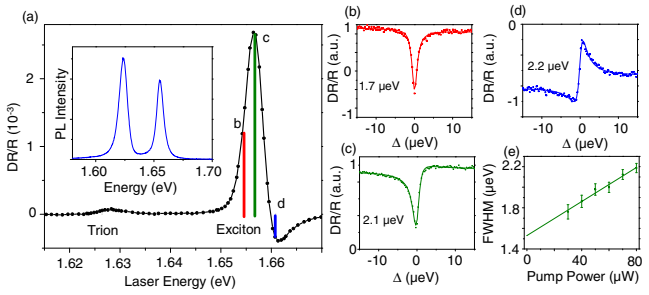


FIG. 2 (color online). (a) Degenerate DR spectrum showing the exciton and trion resonance, consistent with low temperature photoluminescence (PL) measurements (inset). The colored lines indicate the spectral positions of the nondegenerate DR spectra shown on the right. (b)–(d) High resolution nondegenerate DR measurements as a function of pump position [as indicated in inset (a)], showing narrow DR resonances for different pump energies (cross-linearly polarized pump and probe). Linewidths are extracted from fits of a weighted contribution from both the real and imaginary parts of the same complex Lorentzian function. (e) The linewidth is observed to increase linearly with increasing pump power revealing a zero power intercept of $1.53 \pm 0.04$ $\mu$eV and a slope of $8.3 \pm 0.6$ neV/$\mu$W (for 20 $\mu$W probe power at pump position $c$).

measurements on three other $MoSe_2$ monolayers show similar responses [31]. Typical high resolution DR spectra are shown in Figs. 2(b)–2(d) for cross-linearly polarized pump and probe at three different pump energy positions. Each DR spectrum is fit to a weighted sum of the real and imaginary parts of the same complex Lorentzian function ($\beta$) [$A\mathrm{Re}(\beta) + B\mathrm{Im}(\beta)$, where the weights, $A$ and $B$, are allowed to vary]. The Lorentzian linewidth (FWHM) of the resonance is about 2 $\mu$eV. From the low to high energy side of the broad exciton resonance, the linewidth increases by approximately 25%, and an increase of the line shape asymmetry is also observed. A qualitatively similar linewidth dependence has been observed in GaAs quantum well systems, explained by a phonon-assisted spectral diffusion process associated with exciton localization [25]. For the remainder of this work, high resolution DR measurements are performed near or below the exciton line center where the line shape is nearly symmetric.

We examine pump power dependence of the resonance by fixing the pump laser near the peak of the exciton resonance (1.657 eV) and scanning the probe. Figure 2(e) shows the linear dependence of linewidth as a function of pump power at probe power of 20 $\mu$W. Extrapolating to zero pump power, we obtain an intercept of 1.53 $\mu$eV, which is broadened by the probe power. At the lowest applied pump and probe power of 2 $\mu$W, the narrowest observed cross-linearly polarized DR resonance has a linewidth of 0.8 $\mu$eV [blue curve in Fig. 3(a)].

The DR responses show an interesting dependence on polarization (Figs. 3–4). In the first of these measurements, we compare the cross-linearly (blue) and cross-circularly (red) polarized pump and probe. The narrow resonance is negligible in the cross-circularly polarized DR response compared to the cross-linearly polarized response [Fig. 3(a)]. At low power, the cross-linear, co-circular, and colinear polarized responses all have the narrow resonance dip with comparable linewidth (see Fig. 4 and the Supplemental Material [31] for the co-linearly polarized response). Figure 4 shows power dependent DR spectra for both the cross-linearly and co-circularly polarized pump and probe. For the cross-linearly polarized pump and probe [Fig. 4(a)], we observe a broadening of the linewidth with increasing power, consistent with Fig. 2(e), whereas the co-circularly (and co-linearly) polarized spectrum has a qualitatively different line shape [Fig. 4(b)]. Remarkably, for the co-circularly polarized pump and probe, an extremely narrow (<0.2 $\mu$eV FWHM) peak emerges from the dip with increasing laser intensity, eventually dominating the response [Fig. 4(b)].

In a simpler system, such as an inhomogeneously broadened ensemble of two-level atoms, the dominant DR response arises from the third-order susceptibility ($\chi^{(3)}$) when working in the low intensity limit. In a high-resolution pump-probe experiment, narrow resonances in $\chi^{(3)}$ can arise from both incoherent spectral hole burning and coherent contributions from population pulsation [34,35] [Fig. 1(c)]. Hole-burning resonances arise from the saturation of a narrow spectral distribution resulting

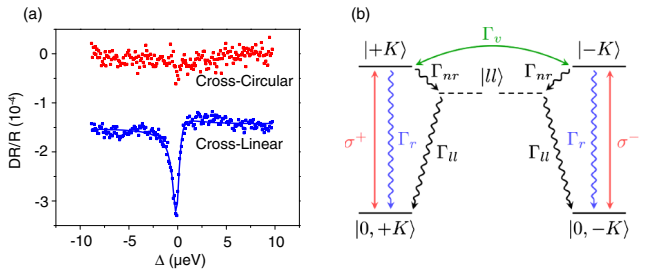


FIG. 3 (color online). Polarization dependent differential reflectivity. (a) The low power (2 $\mu$W pump and probe) DR response has a linewidth of 0.8 $\mu$eV FWHM for cross-linearly polarized pump and probe (blue). The negligible resonance for cross-circularly polarized pump and probe (red) is a consequence of the valley-dependent optical selection rules. The pump energy is 1.655 eV. (b) Energy level diagram of the valley exciton system. Direct exciton transitions occur at $K$ valleys forming two exciton subsystems with $\sigma\pm$ polarized optical selection rules. We model the exciton as a single state for each valley. The exciton relaxation rate ($\Gamma_r$), intervalley relaxation rate ($\Gamma_v$), nonradiative decay rate to long-lived state ($\Gamma_{\mathrm{nr}}$), and long-lived state decay rate ($\Gamma_{\mathrm{ll}}$) are shown.

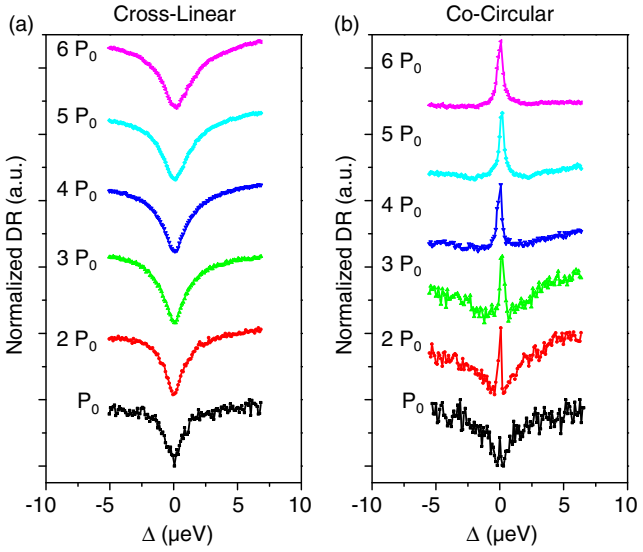


FIG. 4 (color online). Power dependent cross-linear and co-circular differential reflectivity. The reflected pump and probe are simultaneously detected and the two powers are increased together. $P_0$ corresponds to 10 $\mu$W. At $P_0$, the cross-linearly (a) and co-circularly (b) polarized spectra have similar linewidths of 1.8 and 2.5 $\mu$eV, respectively. The amplitude of each spectrum is normalized, and the data are stacked to highlight the changes of line shape with power. The cross-linearly polarized data show a power dependent broadening, consistent with an increase of the nonradiative decay rate, $\Gamma_{\mathrm{nr}}$. At higher powers a narrow peak emerges in the co-circularly polarized spectra whose width is related to the decay rate of the long-lived states, $\Gamma_{\mathrm{ll}}$.

in a decrease in probe absorption around the pump energy. The width of a hole-burning resonance provides a measure of the homogeneous spectral linewidth, including pure dephasing effects. Coherent population pulsation arises from the interference of the pump and probe laser fields through the excitation of the medium, leading to a modulation of the nonequilibrium populations at the pump-probe detuning. The population can follow the temporal modulation provided that the pump-probe detuning is smaller than the state's population decay rate. This coherent process leads to a resonance in the $\chi^{(3)}$ response whose spectral width provides a measure of the state lifetime [34]. Since population pulsation resonances are not directly sensitive to the dephasing rate, they can be orders of magnitude narrower than hole-burning resonances because the dephasing rate is often much larger than the population decay rate in solid state systems. Therefore, population pulsation typically dominates the high resolution $\chi^{(3)}$ response [25]. In a system whose dephasing rate is much larger than a population decay rate, one expects a narrow population pulsation resonance on top of a broad nonlinear signal [25,34].

We attribute the narrow ($\sim$1 $\mu$eV) resonances in DR to coherent population pulsation due to both the narrow linewidths and their polarization dependence [31]. Whereas, the broad DR response likely arises from spectral hole burning that is subject to strong spectral diffusion processes [36]. The nature of this broad nonlinear response will be explored in future work. Our assignments are further supported by recent independent measurements of the exciton homogeneous linewidth in TMD monolayers, which report the linewidth to be on the 1 meV-scale [21], 3 orders of magnitude larger than the $\sim$1 $\mu$eV linewidth of the resonance reported here. We also note that quasi-2D excitons confined to GaAs quantum well structures also exhibited low temperature dephasing rates on the order of 0.5 meV and population pulsation resonance on the $\mu$eV scale [25]. Thus, spectral hole burning is unlikely to be the cause of the narrow resonances.

To understand the population pulsation resonances and their polarization dependence, we use the optical Bloch equations [37] to calculate the nonlinear susceptibility perturbatively in the $\chi^{(3)}$ limit [31]. In monolayer TMDs, we model the valley excitons in the $+K$ and $-K$ valleys as independent subsystems, which are coupled through intervalley relaxation [Fig. 3(b)]. For each valley, we use a single level $|\pm K\rangle$ to denote excitons both inside and outside the light cone [Fig. 3(b)] [31]. We note that this picture can be used as a model for weakly localized excitons. We also phenomenologically include a long-lived state $|ll\rangle$ to account for the extremely narrow linewidth (<0.2 $\mu$eV) peak in the co-circularly polarized response. Possible candidates for such a state include the spin-forbidden or valley-forbidden excitons, and defect trapped states. The valley excitons can relax to such a long-lived state with a rate $\Gamma_{\rm nr}$. In our model, a single rate $\Gamma_r$ accounts for the effective radiative decay rate of the exciton population inside and outside of the light cone [31]. The intervalley relaxation rate of excitons is denoted by $\Gamma_v$. The total decay rate of each valley exciton, $\Gamma_t$ is a sum of $\Gamma_v$,$\Gamma_r$, and $\Gamma_{\rm nr}$. The nonradiative decay rate of the long-lived state is $\Gamma_{\rm ll}$.

The polarization-dependent response can be understood by considering the optical selection rules for bright excitons in monolayer TMDs. Valley excitons in the $+K$ and $-K$ valleys are excited by circularly polarized light with the opposite helicity [38], as shown in Fig. 3(b). Therefore, when both beams are cross-circularly polarized, there should be no population pulsation resonance since the pump and probe fields do not interfere when coupling to excitons in opposite valleys. This explains the negligible dip in the cross-circularly polarized case in Fig. 3(a). Even though the cross-circularly polarized configuration shows a negligible population pulsation response, the broad ($\sim$meV-scale) nonlinear response (away from zero detuning) is similar to the other polarizations, perhaps indicating the importance of intervalley scattering.

The existence of an ultranarrow resonance that distinguishes the cross-linearly and co-circularly polarized DR responses (Fig. 4) can be explained by the optical Bloch equations using the energy model as depicted in Fig. 3(b); however, the sign change of the narrow peak relative to the broader dip requires more complicated theory, which we explore in the Supplemental Material [31]. In the cross-linearly polarized configuration, the interference of the pump and probe fields only modulates the population difference between the $+K$ and $-K$ valley excitons, whereas the sum of the two populations is not modulated [31]. This results in a single Lorentzian in the cross-linearly polarized DR response of the form $1/(\Delta + i\Gamma_t)$, where $\Gamma_t = \Gamma_r + 2\Gamma_v + \Gamma_{\rm nr}$. The pulsation effect from the long-lived state lies in the modulated sum population, and is therefore not present in the cross-linearly polarized measurement. The result of this analysis shows that the narrowest DR resonance in the cross-linearly polarized configuration provides a measure of the exciton average lifetime, which corresponds to the average decay rate $\Gamma_r$ of the bright and dark excitons [31]. An analysis of the role of dark excitonic states is explored in the Supplemental Material [31].

Assuming the usual relationship, $\Gamma^{-1} = \frac{1}{\pi\Delta\nu}$, between lifetime ($\Gamma^{-1}$) and spectral width ($\Delta\nu$), holds for this system, we place a $\sim$1.7 ns lower bound on the lifetime related to the cross-linearly polarized linewidth, $h\Delta\nu \sim$ 0.8 $\mu$eV ($\Delta\nu = 0.19$ GHz) FWHM from Fig. 3(a). Using the model depicted in Fig. 3(b), this rate places a lower bound on the overall exciton lifetime which is 1–3 orders of magnitude longer than the lifetimes recently reported in ultrafast pump-probe experiments [16–20]. We note that the 1.7 ns lifetime corresponds to an average of both the bright and dark exciton lifetimes and includes nonradiative decay to the long-lived state as well as intervalley scattering [31]. The observation of increasing linewidth as

a function of power could indicate the influence of interaction effects [37,39] such as exciton-exciton annihilation [40] [see Fig. 2(e) and Fig. 4], where the power broadening corresponds to a decrease in the exciton lifetime.

When the pump and probe are co-circularly polarized, the fields only couple to bright excitons in one valley. In this case, the interference of the pump and probe fields modulates the exciton population in this valley. The population of the long-lived state is also modulated since it is populated by the relaxation from the $|\pm K\rangle$ exciton. This leads to two types of resonances. The first type is similar to the cross-linearly polarized resonance, whose linewidth is determined by $\Gamma_r$, $\Gamma_v$, and $\Gamma_{\mathrm{nr}}$. The second type of resonance comes from the pulsation of the long-lived state, which contributes an additional resonance proportional to $\Gamma_{\mathrm{nr}}/[(\Delta + i\Gamma_{\mathrm{ll}})(\Delta + i(\Gamma_r + \Gamma_{\mathrm{nr}}))]$. In the limit that the long-lived state decay is slow ($\Gamma_{\mathrm{ll}} \ll \Gamma_r + \Gamma_{\mathrm{nr}}$), the linewidth is given [41] by $\Gamma_{\mathrm{ll}}$. A similar argument can be made for co-linearly polarized excitation [31].

The emergence of the ultranarrow co-circular resonance with increasing intensity can be modeled by phenomenologically adding an exciton density dependence to the nonradiative decay rate $\Gamma_{\mathrm{nr}}$, which increases with exciton density (laser power). With this assumption, the contribution from the long-lived state is negligible at low power excitation. This is consistent with low power (10 $\mu$W) measurements showing similar ($\sim$2 $\mu$eV) linewidths for both cross-linear and co-circular polarizations, which measure $\Gamma_{\mathrm{t}}$. However, under high power (40 $\mu$W) excitation, $\Gamma_{\mathrm{nr}}$ increases, and the long-lived state contribution dominates the co-circularly polarized measurements. We note that recent transient absorption measurements, performed at room temperature on monolayer $MoS_2$, also indicate the importance of density-dependent relaxation phenomena [40].

The narrow peak in the co-circular DR response indicates that the lifetime of the long-lived state is longer than 6.6 ns. The existence of this state, which appears to become more important at higher exciton densities, could be important for interpreting previous time-resolved measurements. For example, if decay to the long-lived state dominates valley exciton relaxation, time-resolved photoluminescence will be rapidly quenched and will effectively measure $\Gamma_{\mathrm{nr}}$, whereas our high resolution coherent nonlinear spectroscopy technique is sensitive to long time scales and ground state dynamics. Relaxation to the long-lived state could also explain the low radiative quantum yield recently reported for monolayer TMDs [1], since the long-lived state can trap the exciton population. This model also gives insight into the recent observation of an increase of exciton lifetime with temperature, since at higher temperature, the long-lived state could scatter back to the bright exciton state by interacting with phonons [16].

We would like to acknowledge useful discussions with D. G. Steel, H. Wang, and Xiaoqin Li. This work is mainly supported by the DOE BES (No. DE-SC0008145 and No. DE-SC0012509). A. M. J. is partially supported by NSF Grant No. DGE-0718124. J. R. is partially supported by NSF Grant No. DGE-1256082. T. K. and K. F. were supported by NSF Grant No. DGE-1256082 and NSF Grant No. 1150647. H. Y. and W. Y. are supported by the Croucher Foundation (Croucher Innovation Award), and the RGC of Hong Kong (HKU705513P, HKU9/CRF/13G). J. Y. and D. M. are supported by US DOE, BES, Materials Sciences and Engineering Division. X. X. thanks the support from the Cottrell Scholar Award. Device fabrication was performed at the University of Washington Nanofabrication Facility and Nanotech User Facility, both members of the NSF National Nanotechnology Infrastructure Network.

*Corresponding author.
xuxd@uw.edu

[1] K. F. Mak, C. Lee, J. Hone, J. Shan, and T. F. Heinz, Phys. Rev. Lett. **105**, 136805 (2010).
[2] A. Splendiani, L. Sun, Y. Zhang, T. Li, J. Kim, C.-Y. Chim, G. Galli, and F. Wang, Nano Lett. **10**, 1271 (2010).
[3] J. S. Ross *et al.*, Nat. Commun. **4**, 1474 (2013).
[4] K. F. Mak, K. L. He, J. Shan, and T. F. Heinz, Nat. Nanotechnol. **7**, 494 (2012).
[5] T. Cao *et al.*, Nat. Commun. **3**, 887 (2012).
[6] H. Zeng, J. Dai, W. Yao, D. Xiao, and X. Cui, Nat. Nanotechnol. **7**, 490 (2012).
[7] A. M. Jones *et al.*, Nat. Nanotechnol. **8**, 634 (2013).
[8] K. F. Mak, K. L. He, C. Lee, G. H. Lee, J. Hone, T. F. Heinz, and J. Shan, Nat. Mater. **12**, 207 (2013).
[9] C. Zhang, A. Johnson, C.-L. Hsu, L.-J. Li, and C.-K. Shih, Nano Lett. **14**, 2443 (2014).
[10] Z. Ye, T. Cao, K. O'Brien, H. Zhu, X. Yin, Y. Wang, S. G. Louie, and X. Zhang, Nature (London) **513**, 214 (2014).
[11] B. Zhu, X. Chen, and X. Cui, arXiv:1403.5108.
[12] A. Chernikov, T. C. Berkelbach, H. M. Hill, A. Rigosi, Y. Li, O. B. Aslan, D. R. Reichman, M. S. Hybertsen, and T. F. Heinz, Phys. Rev. Lett. **113**, 076802 (2014).
[13] K. He, N. Kumar, L. Zhao, Z. Wang, K. F. Mak, H. Zhao, and J. Shan, Phys. Rev. Lett. **113**, 026803 (2014).
[14] G. Wang, X. Marie, I. Gerber, T. Amand, D. Lagarde, L. Bouet, M. Vidal, A. Balocchi, and B. Urbaszek, Phys. Rev. Lett. **114**, 097403 (2015).
[15] M. M. Ugeda *et al.*, Nat. Mater. **13**, 1091 (2014).
[16] T. Korn, S. Heydrich, M. Hirmer, J. Schmutzler, and C. Schüller, Appl. Phys. Lett. **99**, 102109 (2011).
[17] C. Mai, A. Barrette, Y. Yu, Y. G. Semenov, K. W. Kim, L. Cao, and K. Gundogdu, Nano Lett. **14**, 202 (2014).
[18] H. Shi, R. Yan, S. Bertolazzi, J. Brivio, B. Gao, A. Kis, D. Jena, H. G. Xing, and L. Huang, ACS Nano **7**, 1072 (2013).
[19] D. Lagarde, L. Bouet, X. Marie, C. R. Zhu, B. L. Liu, T. Amand, P. H. Tan, and B. Urbaszek, Phys. Rev. Lett. **112**, 047401 (2014).

[20] G. Wang, L. Bouet, D. Lagarde, M. Vidal, A. Balocchi, T. Amand, X. Marie, and B. Urbaszek, Phys. Rev. B **90**, 075413 (2014).
[21] G. Moody *et al.*, arXiv:1410.3143.
[22] H. Wang, C. Zhang, W. Chan, C. Manolatou, S. Tiwari, and F. Rana, arXiv:1409.3996.
[23] H. Wang, C. Zhang, and F. Rana, arXiv:1409.4518.
[24] J. T. Remillard, H. Wang, D. G. Steel, J. Oh, J. Pamulapati, and P. K. Bhattacharya, Phys. Rev. Lett. **62**, 2861 (1989).
[25] H. Wang, M. Jiang, and D. G. Steel, Phys. Rev. Lett. **65**, 1255 (1990).
[26] P.-C. Ku, F. Sedgwick, C. J. Chang-Hasnain, P. Palinginis, T. Li, H. Wang, S.-W. Chang, and S.-L. Chuang, Opt. Lett. **29**, 2291 (2004).
[27] P. Palinginis, S. Tavenner, M. Lonergan, and H. Wang, Phys. Rev. B **67**, 201307 (2003).
[28] M. Lindberg and S. W. Koch, Phys. Rev. B **38**, 3342 (1988).
[29] H. Wang, K. Ferrio, D. G. Steel, Y. Z. Hu, R. Binder, and S. W. Koch, Phys. Rev. Lett. **71**, 1261 (1993).
[30] P. Blake, E. W. Hill, A. H. C. Neto, K. S. Novoselov, D. Jiang, R. Yang, T. J. Booth, and A. K. Geim, Appl. Phys. Lett. **91**, 063124 (2007).
[31] See Supplemental Material at http://link.aps.org/supplemental/10.1103/PhysRevLett.114.137402, which includes Refs. [32,33], addition data taken on other samples and co-linearly polarized measurements. It also contains a detailed theoretical analysis of the DR response.
[32] M. Benameur, B. Radisavljevic, J. Heron, S. Sahoo, H. Berger, and A. Kis, Nanotechnology **22**, 125706 (2011).
[33] E. J. Sie, Y.-H. Lee, A. J. Frenzel, J. Kong, and N. Gedik, arXiv:1312.2918.
[34] Y.-R. Shen, *The Principles of Nonlinear Optics* (Wiley-Interscience, New York, 1984).
[35] P. R. Berman and V. S. Malinovsky, *Principles of Laser Spectroscopy and Quantum Optics* (Princeton University Press, Princeton, 2010).
[36] H. Wang and D. G. Steel, Phys. Rev. A **43**, 3823 (1991).
[37] G. Rochat, C. Ciuti, V. Savona, C. Piermarocchi, A. Quattropani, and P. Schwendimann, Phys. Rev. B **61**, 13856 (2000).
[38] D. Xiao, G.-B. Liu, W. Feng, X. Xu, and W. Yao, Phys. Rev. Lett. **108**, 196802 (2012).
[39] M. Mittendorff *et al.*, Nat. Phys. **11**, 75 (2015).
[40] D. Sun, Y. Rao, G. A. Reider, G. Chen, Y. You, L. Brézin, A. R. Harutyunyan, and T. F. Heinz, Nano Lett. **14**, 5625 (2014).
[41] D. G. Steel, S. C. Rand, and J. Liu, J. Opt. Soc. Am. B **4**, 1794 (1987).